A High Intensity Focused Ultrasound System for Veterinary Oncology Applications

Kyriakos Spanoudes[1,2], Nikolas Evripidou[1], Marinos Giannakou[3], Theocharis Drakos[1,3], George Menikou[4], Christakis Damianou[1]*

[1]Department of Electrical Engineering, Cyprus University of Technology, Limassol, Cyprus, [2]Vet Ex Machina Ltd., Nicosia, Cyprus, [3]Medsonic Ltd., Limassol, Cyprus, [4]Medical Physics Sector, General Hospital of Nicosia, Nicosia, Cyprus

Abstract

Background: Magnetic resonance-guided focused ultrasound surgery is an incisionless energy-based thermal method that is used for ablating tumors in the veterinary clinic. **Aims and Objectives:** In this article we describe a prototype of a veterinary system compatible with magnetic resonance imaging intended for small-to-medium-sized companion animals that was developed and tested in vivo in adult rabbits. **Methods:** Real-time monitoring of the ablation during the experiment was possible with MR thermometry. Experiments involved thermal monitoring of sonications applied in the thigh of the rabbits. A 38-mm diameter transducer operating at 2.6 MHz was used with a 60-mm-focal length. The robotic system employed 3 linear axes and one angular axis. For this study, only X and Y axis were enabled. Due to the target size limitations, motion in Z and Θ was not needed. The functionality of the positioning device was evaluated by means of MR thermometry, demonstrating sufficient heating and accurate motion in both axes of operation. **Results:** The postmortem findings confirm the ability of the system to induce thermal ablations in vivo in the absence of adverse effects. **Conclusions:** The device is a reliable and affordable solution for companion animal hospitals, offering and additional tool for the veterinary oncology society.

Keywords: Rabbit, ultrasound, veterinary oncology

INTRODUCTION

It is widely accepted among the international veterinary society that animal oncology care is significantly falling behind human oncology. While targeted therapies, immunotherapies, and sophisticated interventional techniques are routinely available for humans, a fraction of animal oncology cases have access to the now traditional treatments such as chemotherapy and radiation therapy, while referral culture is not fully developed.[1] It is also an undisputable fact that veterinary medicine adopts therapies, long after they are validated and established in human medicine, such as immunotherapies[2] and small molecule inhibitors.[3] Research in the veterinary field has the potential to change the dynamics of this imbalanced relationship, which will benefit both animals and humans. Due to a largely common genetic, molecular and histological background, studies in dogs have facilitated the translation of cancer trials to humans.[4] Notably, these studies have successfully answered research questions, where mice and human trials failed.[5] These advancements have been materialized partially due to the increased availability of affordable genomic and molecular characterization; bringing precision cancer medicine a step closer to veterinary clinics.[6] The benefits of these studies not only promote the veterinary oncology field but also benefit humankind, making companion animals valuable partners for translational science.[7] It is worth noting that taking the example of human clinical trials and running multicenter, double-blinded trials to compare existing and novel therapies would enhance the credibility of thereof. However, the logistics and economics of veterinary medicine currently preclude this practice in large scale. Nevertheless, carefully designed studies should be adopted to comply with the ethical parameters of studies *in vivo*.[8]

Address for correspondence: Prof. Christakis Damianou, Department of Electrical Engineering, Cyprus University of Technology, Limassol, Cyprus.
E-mail: christakis.damianou@cut.ac.cy

Magnetic resonance-guided focused ultrasound surgery (MRgFUS) is an incisionless energy-based thermal method to ablate tumors. Up to date, its use has been reported for the treatment of prostate,[9,10] bone metastases,[11] pancreas,[12] liver,[13] and uterine fibroids.[14] It is among the modalities currently investigated for tumor ablation in veterinary medicine.[15] Currently, only a handful of veterinary hospitals are utilizing MRgFUs for veterinary medicine applications. The scarcity of MRgFUs veterinary centers can be attributed to a number of reasons such as the lack of affordable devices for treatment, the small number of dedicated animal magnetic resonance imaging (MRI) imaging centers where MRI-guidance is an absolute requirement, the limited evidence-based literature in the field, and the lack of interest by MRgFUs vendors to invest and expand in the field of veterinary medicine.

Following prostate treatment advancements in human oncology, analogous companion animal studies have been conducted to investigate the potential of the technology for prostate therapies.[16-22] A study focusing on naturally occurring solid tumors in canines such as in urinary bladder, oral cavity, hip, mammary gland, orbits, and abdominal cavity, demonstrated a significant decrease in tumor size in some and a noticeable clinical improvement (cessation of bleeding) in subjects with hemorrhagic tumors.[23] In another study, MRgFUS was successful in ablating significant volumes of hepatocellular adenomas in four canines,.[24] Interestingly, the technique is also finding application as a part of novel therapy in combination with advanced therapeutics, such as an anticancer micelle.[25] It is of paramount importance that MRgFUS is becoming a drug delivery component, where it can be utilized as a remote switch for targeted delivery of molecules. These advancements will reveal the full potential of the technique in the stage of advanced oncology therapeutics.

In ophthalmology, the hypotensive effect of high-intensity focused ultrasound (HIFU) in managing intraocular pressure in dogs with primary glaucoma was demonstrated successfully without observing intra-operative complications.[26] The technique has also been tested with promising results in interventional cardiology strategies such as for managing ventricular arrhythmia,[27,28] cardiac ablation,[29,30] and atrial fibrillation treatment.[31,32] The effectiveness of HIFU in treating drug-resistant hypertension via bilateral renal nerves ablation was investigated in canine models.[33] The study reported an effective renal sympathetic denervation confirmed by histology that resulted in an improvement in renal function. Another study initially utilized a model of hypersplenism and was tested in secondary cases of splenomegaly.[34] Apart from medical and surgical pathologies, the technique has been proposed as a noninvasive neutering method for male contraception.[35,36]

In our work, a novel MRgFUS system for veterinary applications was presented. The proposed system is nonmagnetic and thus fully compatible with any commercial 1.5T MRI. The robotic system is highly customizable offering up to 4 degrees of freedom (X, Y, Z, and Θ axes) depending on the intended use of the device. A custom-made platform is designed to controls the positioning device and the sonication parameters of the ultrasound system. The robotic device is compact (44 cm in length, 14.7 cm in width, and 6.15 cm in height) and ergonomic. The device is carrying a single element transducer, which translates into a cost-effective solution for the veterinary market. In this *in vivo* feasibility study with rabbits, the following aspects of the device were investigated: (1) The coupling efficiency to allow safe and efficient ablation, (2) The positioning device's movement accuracy in standard operating conditions, (3) Animal placement and immobilization for the procedure, (4) The transducer efficiency to create both discrete and overlapping lesions.

MATERIALS AND METHODS

Mechanical design of the positioning device

The positioning device includes four computer-controlled axes (X, Y, Z and Θ). Figure 1 shows the CAD drawings of the robotic system. The moving plate of each axis is coupled to a threaded plastic screw which was attached directly to the shaft of a piezoelectric motor (USR 30-S3, Shinsei Kogyo Corp., Tokyo, Japan). The rotation of the shaft converts the angular motion to the linear translation of the plate. An encoder plastic strip is attached on the axis frame and scanned by an encoder module (US Digital Corporation, Vancouver, WA 98684, USA) provides in real-time displacement feedback to the control platform. The encoder module EM1-0-500-I (US Digital Corporation, Vancouver, WA 98684, USA) was used for all three linear axes. For the theta axis, which is coupled directly on the motor's shaft, an EM1-2-2500-I (US Digital Corporation, Vancouver, WA 98684, USA) encoder was used. The encoder output is connected to the counter input of a data acquisition board USB 6251 (National instruments, Austin, Texas, USA). Images of the developed robotic system are shown in Figure 2.

Compared to our previous animal positioning device,[37] the main difference is the size of the motors, which is significantly smaller in the new design (almost 50% smaller), allowing the development of a more compact positioning device. The transducer is immersed in a separate watertight compartment of the device, which is filled with degassed water.

The transducer's active element consisted of a P762-type piezoceramic crystal (Piezohannas Tech. Co., Wuhan, China). Epoxy capable of withstanding temperatures up to 100°C without losing its integrity was used as a backing material of the transducer element. The transducer's impedance was matched to 50 Ω. To reduce the transmission of high-frequency harmonics, a custom made low-pass filter was used (10 MHz cut-off frequency).

The positioning device was modeled using CAD software (Microstation V8, Bentley Systems, Inc., Beijing, China). The positioning device's parts were fabricated using fusion deposition modelling technology (FDM400, Stratasys, Eden Pairie, Minnesota, USA) that employed acrylonitrile butadiene styrene filament.
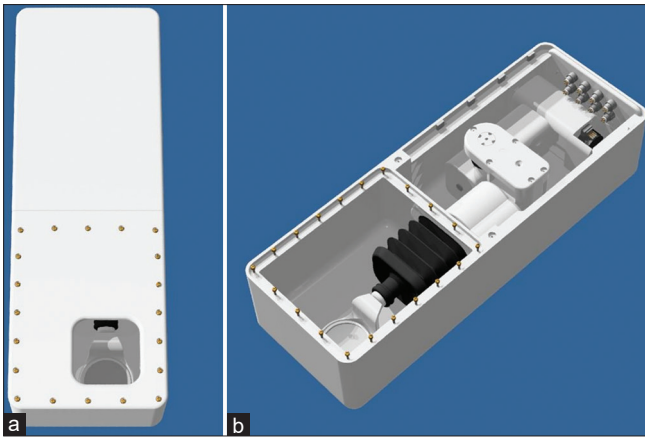
Figure 1: (a) External CAD drawing of the robotic system. (b) Internal CAD drawing of the robotic system

Figure 2: (a) Photo of the developed robotic system. (b) Photo of the rabbit placement for procedure on the robotic system

Software

The positioning device is controlled via an in-house developed user-friendly program developed in C # (Visual Studio 2010 Express, Microsoft Corporation, Redmond, USA). The software holds the following functionalities: (a) Communication with MRI, (b) 2 axes movement either manually or automatically by specifying the algorithm,[38] the step and the number of steps, (c) MR thermometry, and (d) Ultrasound control (frequency, power, sonication time, and cooling time).

Electronic system

The motor drivers were hosted in a metallic enclosure placed outside the MRI room. The enclosure includes a DC supply (24 V, 2 A), which drives the Shinsei motors. Wires connect the motor drivers and a data acquisition interface card (USB 6251, NI) via a connecting block. The USB 6251 interface card includes the timing and digital I/O modules. The motors are driven in clockwise rotation when the ground and clockwise terminals of the motor drivers are connected to the same potential or in the anti-clockwise rotation when the ground and anti-clockwise terminals of the motor drivers are connected to the same potential.

Magnetic resonance-guided-focused ultrasound surgery system

The proposed MRgFUS system is modular system composed of the positioning device described above, a signal generator (HP 33220A, Agilent technologies, Englewood, CO, USA), an RF amplifier (Model: BT00250-AlphaS-CW, Tomco Technologies, Stepney, Australia) and a spherical transducer made from piezoelectric ceramic (Ferroperm). The transducer operates at 2.578 MHz, has focal length of 60 mm and diameter of 38 mm.

In vivo study

The experimental protocol was approved by the Animal Welfare Committee of the Veterinary Services, Ministry of Agriculture, Republic of Cyprus (CY/EXP/PR.L6/2019). Ten female locally bred rabbits provided by an approved vendor were included in the stud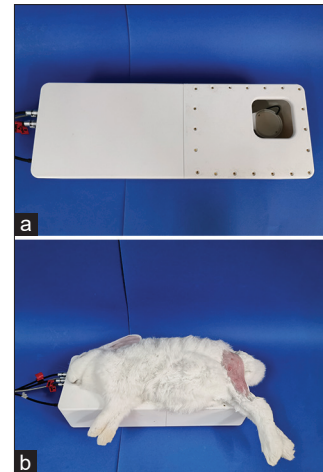y. A qualified veterinary surgeon was assigned to continuously monitor the vital signs of the animals throughout the experiment. The rabbits underwent injectable anesthesia with the combined intramuscular administration of 0.5 mg/kg medetomidine (Medeson, Invesa SA, Barcelona, Spain) and 0.15 mg/kg Ketamine (Narketan-10, Vetoquinol LTD, Towcester, UK). The thighs of the rabbit were depilated (VEET, Reckitt Benkiser, Slough, UK), and the rabbit was placed on the platform with its thigh immersed in the degassed water above the transducer. Upon completion of the experimental procedure, the animals were humanely euthanized with intracardial injection of an agent containing embutramide, mebezonium, and tetracaine (T61, MSD Animal Health, Madison, USA). The tissues of the animals were dissected postmortem for macroscopic observation and measurements.

X-ray imaging

X-rays were taken prior treatment with an X-ray system (IMS001, Shenzhen Browiner Tech Co., Ltd, Shenzhen, China). The animal was set on left recumbency above a CR (Computed Radiography) cassette. On taking the X-ray, the latent image of the cassette was digitized with a CR reader (Vita Flex, Carestream Health, Inc., NY, USA). The purpose of the X-ray taken was to estimate the available muscle area for ablation with dedicated software (Carestream image suite, Carestream Health, Inc., NY, USA).

Magnetic resonance imaging

For the real-time assessment of tissue ablation *in situ,* the full procedure was run on the anesthetized rabbit while being tested in a 1.5 T MR system (Signa Excite 1.5 T, by General Electric, Fairfield, CT, USA). High-resolution MRI was performed to visualize the animal/transducer setup. Thus, a T2-weighted fast spin-echo sequence was used with the following parameters: Repetition time (TR) was 2500 ms, echo time (TE) was 60 ms, slice thickness was 3 mm (gap 0.3 mm), matrix 256×256, field of view (FOV) was 16 cm, the number of excitations (NEX) was 3, while echo train length (ETL) was 8.

Magnetic resonance thermometry

Temperature maps were reconstructed in quasi real time after data processing. Image data were acquired in the coronal plane using echo-planar imaging (EPI) single-shot sequences for monitoring sonications of 23 W acoustic power. The main scanning parameters used to obtain these images were: TE: 24 ms, TR: 80 ms, NEX: 8, ETL: 1, FOV: 20 cm, slice thickness: 3 mm, while flip angle was 25°.

Temperature increment during thermal ablation was estimated using the proton resonance frequency shift equation as described in detail.[39] The equation relates to the measured MR signal's phase shift with temperature elevation (ΔT). This relationship is given by:

$$\Delta T = \frac{\varphi(T) - \varphi(T_0)}{\gamma \alpha B_0 TE}$$

where $\phi(T_0)$ and $\phi(T)$ are the phases at a starting and final temperature T_0 and T, respectively, γ is the gyromagnetic ratio
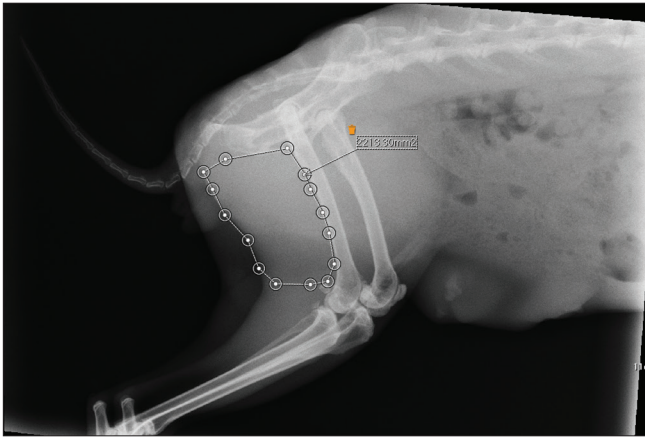

Figure 3: Radiography of a rabbit thigh and calculation of the muscle area reveals the tissue available for ablation
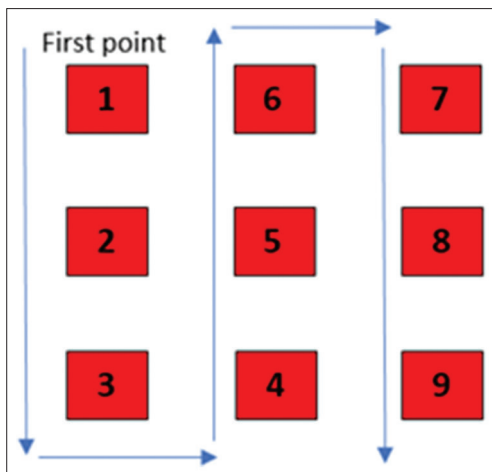

Figure 5: Pathway of the grid pattern that was performed on the rabbit's thigh. A 3 × 3 grid pattern with 5 mm spacing and a cooling time of 140 s. Between ablations was followed. Ablation settings: f = 2.578 MHz, Acoustic Power = 27 W, focal depth = 10 mm, sonication time = 60 s)

in MHz/T, α is the PRF change coefficient in ppm/°C, B_0 is the magnetic field strength in T and TE is the echo time.

RESULTS

As shown in Figure 3, X-ray imaging of the rabbit thigh, and demarcation of the muscle tissue, supported calculation of area available for thermal ablation. The thigh area ranged from 21 cm² to 30 cm² with an average of 25.57 cm² and standard deviation of 3.16 cm².

High-intensity sonications were able to produce 5-mm diamater discrete lesions, as shown in Figure 4a. These lesions are shown in a plane perpendicular to the ultrasound beam. Settings: Acoustic Power was set at 15.64 W, focal depth at 10 mm and sonication time was 30 s. The lesion length varied from 12 mm to 15 mm with an average of 13.5 mm and a standard deviation of 1.5 mm. Figure 4b shows the same discrete lesions after dissection. These lesions are shown in a plane parallel to the ultrasound beam. Settings: Acoustic Power was set at 15.64 W, focal depth at10 mm and sonication time was 30 s. The lesion length varied from 12 mm to 15 mm with an average of 13.5 mm and standard deviation of 1.5 mm.

The designed pathway of the grid pattern is shown in Figure 5. Each numbered point corresponds to an ablation site, 5 mm apart. Sonication time was 30 s and cooling time was 60 s.
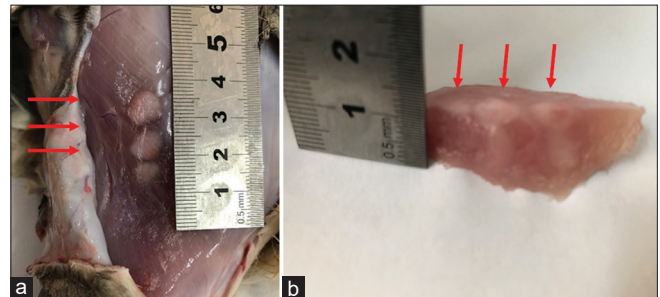

Figure 4: (a) Macroscopic appearance of discrete lesions inflicted by ablation with the system demonstrating: (a) The lesion size in a plane perpendicular to the transducer. (b) The lesion after dissection in a plane parallel to the transducer (f = 2.578 MHz, Acoustic Power = 15.64 W, focal depth = 10 mm, sonication time = 30 s) Red arrows indicate lesions
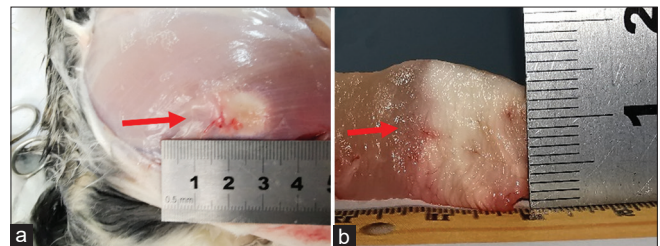

Figure 6: (a) Macroscopic appearance of overlapping lesions inflicted by ablation with the FUSROBOT system demonstrating the lesion size in a plane perpendicular to the transducer. (b) The lesions after dissection in a plane parallel to the transducer. Ablation settings: f = 2.578 MHz, acoustic power = 29.9 W, focal depth = 20 mm, sonication time = 30 s. A 3 × 3 grid pattern with 5 mm spacing and a cooling time of 140 s. Between ablations was followed. Red arrow indicates lesions

Figure 6a shows overlapping lesions created with a series of high intensity sonications. These lesions are shown in a plane perpendicular to the ultrasound beam. Settings: Acoustic Power was set at 29.9 W, focal depth was 10 mm, sonication time at 30 s. A 3 × 3-point grid with 60 s cooling time between successive ablations was followed. Figure 6b shows the same overlapping lesions after dissection. These lesions are shown in a plane parallel to the ultrasound beam. Settings: Acoustic

Power was set at 29.9 W, focal depth was 10 mm, sonication time at 30 s. A 3 × 3-point grid with 60 s. Cooling time between ablations was followed. The overall diameter of the overlapping lesions was 20 mm, while the lesion length was 14 mm.

Temperature maps reconstructed after data processing and which were obtained in the coronal plane are demonstrated in Figure 7a. Settings: Acoustic power was set *at* 27 W, focal depth was 20 mm sonication time of 10 s, 20 s, 30 s, 40 s,
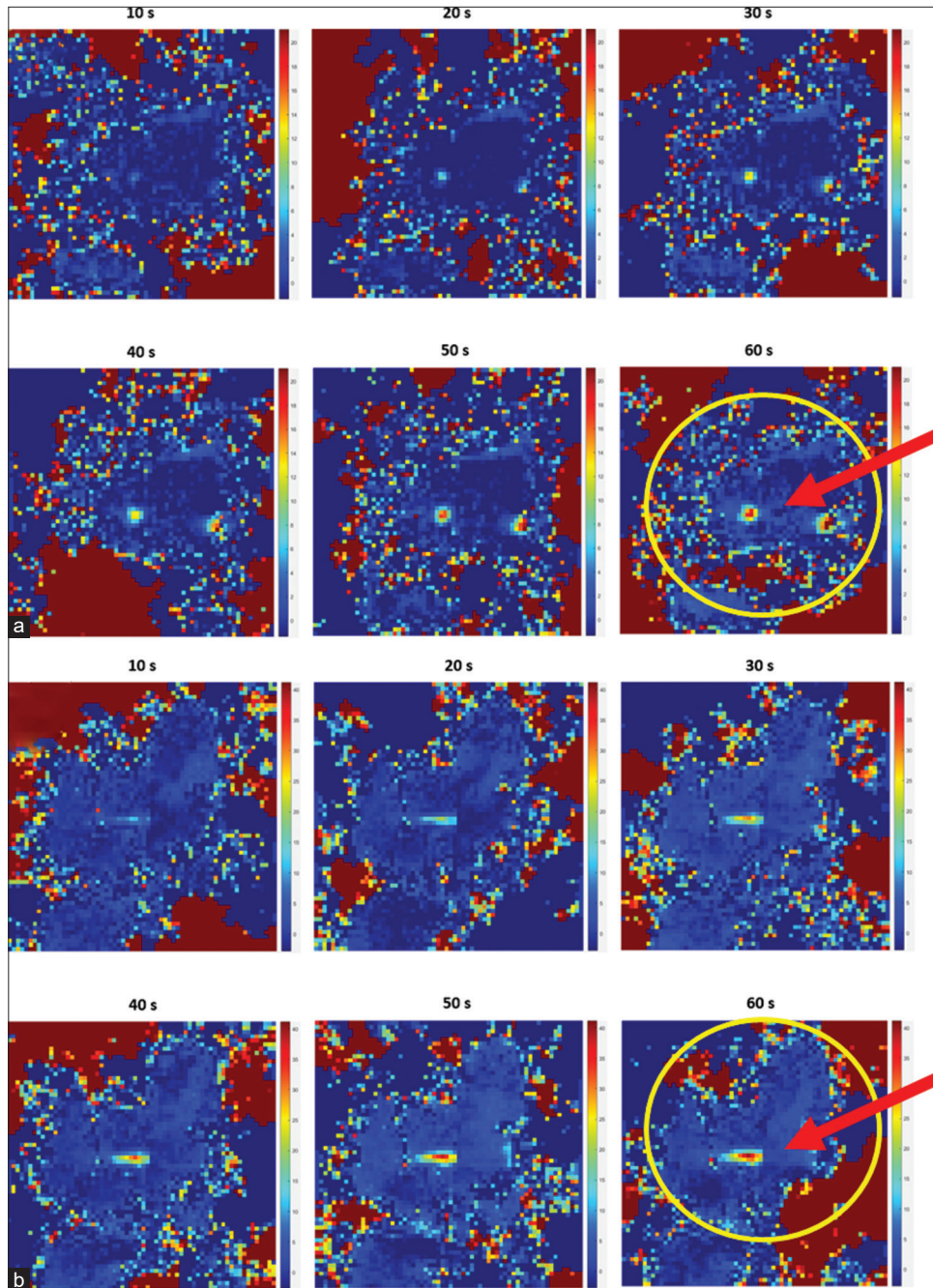

Figure 7: (a) Temperature maps (coronal plane) recorded using single shot echo-planar imaging sequence for sonication of 10 s, 20 s, 30 s, 40 s, 50 s and 60 s. MR parameters: Number of excitations = 8, TR = 80 ms, TE = 24 m. Yellow circle indicates the rabbit thigh. Red arrow indicates lesion. (b) Temperature maps (sagittal plane) recorded using single shot echo-planar imaging sequence and the transducer. Acquisition time of each image = 1.64. Ablation settings: f = 2.578 MHz, Acoustic Power = 27 W, focal depth = 20 mm) for sonication of 10 s, 20 s, 30 s, 40 s, 50 s and 60 s. s. Yellow circle indicates the rabbit thigh. Red arrow indicates lesion

50 s, and 60 s using single-shot EPI gradient echosequence. MR parameters: NEX: 8, TR: 80 ms, TE: 24 ms, temporal resolution of the sequence was 1.64 s/image. The temperature change recorded at 60 s was 17.06°C. Figure 7b shows the temperature maps reconstructed after data processing and which were obtained in the sagittal plane. Settings: Acoustic power was set at 27 W, focal depth was 20 mm sonication *time* of 10 s, 20 s, 30 s, 40 s, 50 s, and 60 s. Within the rabbit using EPI single-shot sequence. MR parameters: NEX: 8, TR: 80 ms, TE: 24 ms, was temporal resolution of the sequence was 1.64 s/image. The temperature change recorded at 60 s was 39.59°C.

Coronal MR images with T2-weighted fast spin-echo sequence with the following parameters: TR: 2500 ms, TE: 60 ms, slice thickness: 3 mm (gap 0.3 mm), matrix 256 × 256, FOV: 16 cm, NEX: 3, and ETL: 8. Settings: Acoustic Power was set at 27 W, focal depth was 20 mm, sonication time at 60 s. A 3 × 3-point grid with 140 s cooling time between successive ablations was followed. The lesions appear in a plane perpendicular to the beam. The dimensions of the ablated area were 20 × 25 mm, while the lesion length was 24 mm [Figure 8].

A T2-weighted fast relaxation fast spin-echo (T2W-FRFSE) coronal image with fat suppression was acquired after the grid pattern to observe the ablated area [Figure 9a]. The dimensions of the ablated area were 2.17 cm × 1.84 cm. Settings: Acoustic power was set at 27 W, focal depth was 20 mm, sonication time at 60 s. A 3 × 3-point grid with 140 s. Cooling time between successive ablations was followed. Figure 9b shows a T2W-FRFSE axial image with fat suppression was acquired after the grid pattern to observe the ablated area. Settings: Acoustic Power was set at 27 W, focal depth was 20 mm, sonication time at 60 s. A 3 × 3-point grid with 140 s. Cooling time between successive ablations was followed. The dimensions of the ablated area are 26.8 mm × 29.8 mm.

Figure 10a demonstrates the corresponding tissue damage induced by ablation under MR imaging, as described in Figure 8. Settings: Acoustic Power was 27 W, focal depth
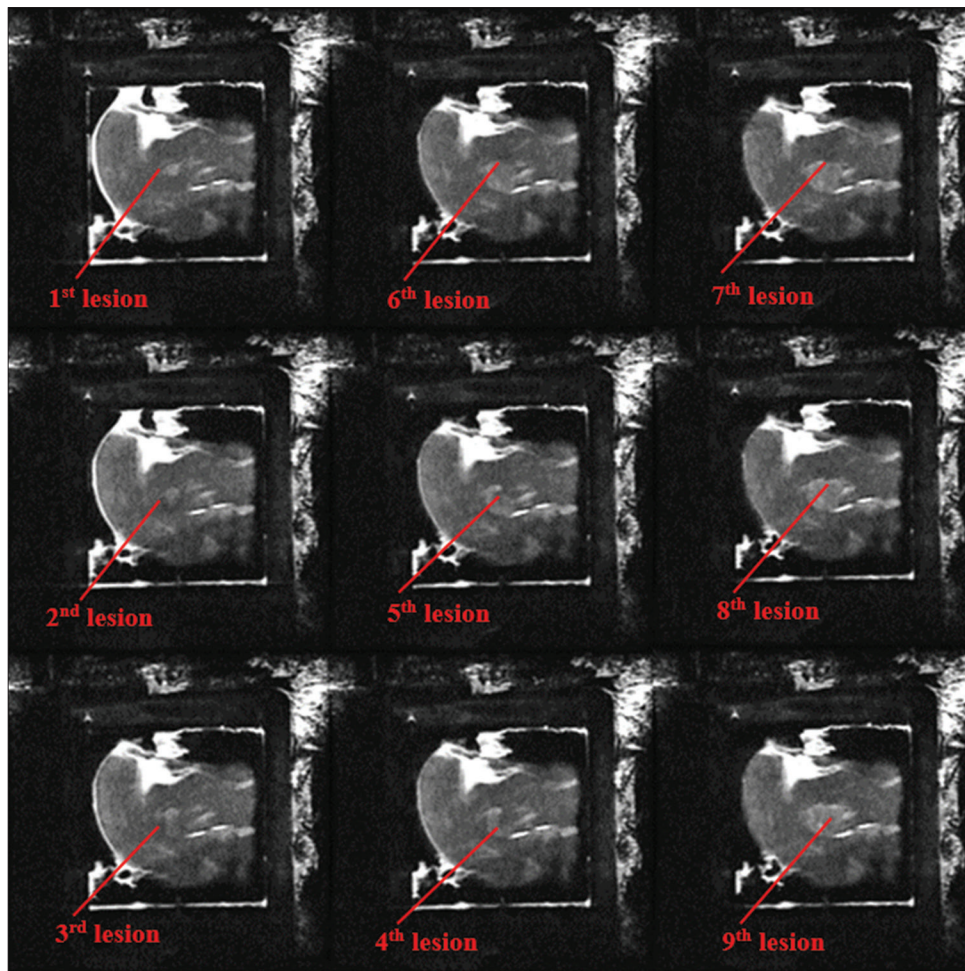

Figure 8: Coronal magnetic resonance images showing lesions with T2W-weighted fast spin echo sequence was used with the following parameters: TR = 2500 ms, TE = 60 ms, slice thickness = 3 mm (gap 0.3 mm), matrix = 256 × 256, field of view = 16 cm, number of excitations = 3, echo train length = 8. Ablation settings: Frequency = 2.578 Mhz, acoustic power = 27 W, focal depth = 20 mm, sonication time = 60 s. A 3 × 3 grid pattern with 5 mm spacing and a cooling time of 140 s. Between ablations was followed. The lesions appear in a plane perpendicular to the beam
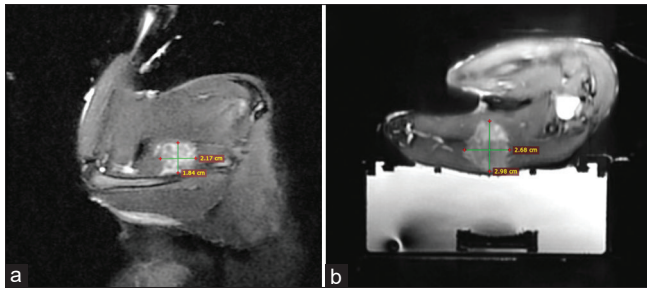
Figure 9: (a) Coronal T2-weighted fast relaxation fast spin-echo image with fat suppression that was obtained after the completion of the ablation plan. (b) Axial T2-weighted fast relaxation fast spin-echo image with fat suppression that was obtained after the completion of the ablation plan

Figure 10: (a) Macroscopic appearance of discrete lesions after dissection inflicted by ablation with the system in a plane perpendicular to the transducer. (b) Dissected tissue of the ablated area that was created. Ablation settings: $f = 2.578$ MHz, acoustic power of 27 W focal depth 20 mm, sonication time was 60 s. A 3×3 grid pattern with 5 mm spacing and a cooling time of 140 s. between ablations was followed. The lesions appear in a plane parallel to the transducer. Red square indicated area of lesions; Red arrow indicates lesion

was 20 mm, sonication time was 60 s. with 140 s. The cooling time between ablations. The lesions appear in a plane perpendicular to the beam. The dimensions of the ablated area were 20 mm × 25 mm. Figure 10b demonstrates the same lesions after dissection. These lesions are shown in a plane parallel to the ultrasound beam. The lesion length was 24 mm.

DISCUSSION

The proposed device is capable of producing both discrete and overlapping lesions in the healthy muscle tissue of rabbits. The software and the positioning apparatus are moving the transducer with accuracy to the location selected by the user. The depth of the lesion corresponds with the focal depth of the transducer element. The accuracy of the device to ablate tissue is confirmed both by real-time MR imaging and postmortem dissection. A reliable MRgFUs system, compatible with multiple MR systems, will offer a solution for incisionless intervention for tumor ablation in veterinary hospitals. Its utilization can be of therapeutic or palliative intent. Tumors of superficial tissues such as the integumentary system, skeletal structures, mammary and testicular glands can be ablated with precision with minimal animal discomfort in the clinic. Such tumors can be ablated under ultrasound guidance from skilled surgeons without the need of MRI guidance. Tumors of the alimentary, reproductive, lymphatic, circulatory system require MRI guidance; however, general anesthesia for such a procedure does not exceed the time of surgery and does not carry the risks associated with surgery complications (i.e., hemorrhage, infection, and thrombosis).

Contrary to human medicine, the treatment cost is a major factor that drives decision-making in Veterinary medicine. It is, therefore, important that a newly launched technology will be affordable to become available in companion animal hospitals. The proposed system has been designed with the intention to be affordable for most referral veterinary hospitals with an existing MRI system in place. The investment required is reduced not only due to its compatibility with multiple MRI systems but also because it carries a single-element transducer. More specifically, the system requires a laptop compu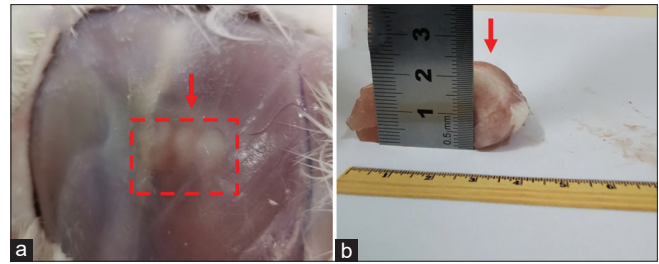ter to carry the software, a bed modification to host the robotic system, while no upgrade is required for the MRI system. In a future study, we will assess the efficacy of the system to ablate naturally occurring tumors of companion animals. The disease recurrence and patient survival of treated patients need to be compared to those achieved with chemotherapy and radiation. In addition, the system can be tested not only as a stand-alone option but also in combination with other modalities (chemotherapy, targeted therapies, and immunotherapies). The technology is also expected to play a major role in drug delivery applications for cancer. Overall, MRgFUs is a promising technology that will be influencing cancer therapeutics for the years to come.

CONCLUSIONS

This study demonstrated the capability of the proposed system of thermally ablating in a controllable and reproducible manner. Tissue ablation remained within the targeted zone, sparing normal surrounding tissue in the absence of adverse effects. In accordance with the designed focal depth of the device, no major cutaneous tissue lesion was observed during the procedure. MRgFUs is designed to target tumors avoiding bone structures in the path of the beam. In addition, during the procedure, there was neither evidence of animal distress nor reaction, suggesting that under the proper anesthetic regime, the welfare of the animal is not compromised.

The system used in this experiment has shown to be capable of producing ablations in healthy tissue *in vivo.* Under MR guidance, the system can ablate tissues in depth with precision and efficiency. MRI enabled near real-time temperature monitoring of the treatment.

Financial support and sponsorship

Conflicts of interest
There are no conflicts of interest.

References

1. Kidd C. The many challenges of veterinary oncology. Can Vet J 2008;49:1132-5.
2. Dow S. A role for dogs in advancing cancer immunotherapy research. Front Immunol 2019;10:2935.
3. Londhe P, Gutwillig M, London C. Targeted therapies in veterinary oncology. Vet Clin North Am Small Anim Pract 2019;49:917-31.
4. Paoloni M, Khanna C. Translation of new cancer treatments from pet dogs to humans. Nat Rev Cancer 2008;8:147-56.
5. Khanna C, Lindblad-Toh K, Vail D, London C, Bergman P, Barber L, *et al*. The dog as a cancer model. Nat Biotechnol 2006;24:1065-6.
6. Katogiritis A, Khanna C. Towards the delivery of precision veterinary cancer medicine. Vet Clin North Am Small Anim Pract 2019;49:809-18.
7. Kol A, Arzi B, Athanasiou KA, Farmer DL, Nolta JA, Rebhun RB, *et al*. Companion animals: Translational scientist's new best friends. Sci Transl Med 2015;7:308ps21.
8. Yeates JW. Ethical principles for novel therapies in veterinary practice. J Small Anim Pract 2016;57:67-73.
9. Ghai S, Perlis N, Lindner U, Hlasny E, Haider MA, Finelli A, *et al*. Magnetic resonance guided focused high frequency ultrasound ablation for focal therapy in prostate cancer – Phase 1 trial. Eur Radiol 2018;28:4281-7.
10. Bass R, Fleshner N, Finelli A, Barkin J, Zhang L, Klotz L. Oncologic and functional outcomes of partial gland ablation with high intensity focused ultrasound for localized prostate cancer. J Urol 2019;201:113-9.
11. Harding D, Giles SL, Brown MR, Ter Haar GR, van den Bosch M, Bartels LW, *et al*. Evaluation of quality of life outcomes following palliative treatment of bone metastases with magnetic resonance-guided high intensity focused ultrasound: An international multicentre study. Clin Oncol (R Coll Radiol) 2018;30:233-42.
12. Marinova M, Rauch M, Mücke M, Rolke R, Gonzalez-Carmona MA, Henseler J, *et al*. High-intensity focused ultrasound (HIFU) for pancreatic carcinoma: Evaluation of feasibility, reduction of tumour volume and pain intensity. Eur Radiol 2016;26:4047-56.
13. Luo Y, Jiang Y. Comparison of efficiency of TACE plus HIFU and TACE alone on patients with primary liver cancer. J Coll Physicians Surg Pak 2019;29:414-7.
14. Laughlin-Tommaso S, Barnard EP, AbdElmagied AM, Vaughan LE, Weaver AL, Hesley GK, *et al*. FIRSTT study: Randomized controlled trial of uterine artery embolization vs focused ultrasound surgery. Am J Obstet Gynecol 2019;220:174.
15. Culp WT, Griffin MA. Veterinary clinics: Tumor ablation. Vet Clin North Am Small Anim Pract 2019;49:949-66.
16. Burtnyk M, Hill T, Cadieux-Pitre H, Welch I. Magnetic resonance image guided transurethral ultrasound prostate ablation: A preclinical safety and feasibility study with 28-day followup. J Urol 2015;193:1669-75.
17. Darnell SE, Hall TL, Tomlins SA, Cheng X, Ives KA, Roberts WW. Histotripsy of the prostate in a canine model: Characterization of post-therapy inflammation and fibrosis. J Endourol 2015;29:810-5.
18. Lake AM, Hall TL, Kieran K, Fowlkes JB, Cain CA, Roberts WW. Histotripsy: Minimally invasive technology for prostatic tissue ablation in an *in vivo* canine model. Urology 2008;72:682-6.
19. Lu J, Ye Z, Wang W, Chen Z, Zhang Y, Hu W. Experimental study on the effect of high-intensity focused ultrasound (HIFU) using Sonablate-500 in the ablation of canine prostate. J Huazhong Univ Sci Technol 2007;27:193-6.
20. Pauly KB, Diederich CJ, Rieke V, Bouley D, Chen J, Nau WH, *et al*. Magnetic resonance-guided high-intensity ultrasound ablation of the prostate. Top Magn Reson Imaging 2006;17:195-207.
21. Yoo DH, Cho JY, Kwak C, Lee JY, Moon KC, Kim SH. Transabdominal high-intensity focused ultrasound therapy of the prostate and determination of the protective effect of rectal cooling: An experimental study using canine prostates. J Ultrasound Med 2013;32:1419-25.
22. Zhang J, Wu S, Liu Y, Qiao L, Gao W, Zhang W, *et al*. Disruption of prostate microvasculature by combining microbubble-enhanced ultrasound and prothrombin. PLoS One 2016;11:e0162398.
23. Ryu MO, Lee SH, Ahn JO, Song WJ, Li Q, Youn HY. Treatment of solid tumors in dogs using veterinary high-intensity focused ultrasound: A retrospective clinical study. Vet J 2018;234:126-9.
24. Kopelman D, Inbar Y, Hanannel A, Dank G, Freundlich D, Perel A, *et al*. Magnetic resonance-guided focused ultrasound surgery (MRgFUS). Four ablation treatments of a single canine hepatocellular adenoma. HPB (Oxford) 2006;8:292-8.
25. Horise Y, Maeda M, Konishi Y, Okamoto J, Ikuta S, Okamoto Y, *et al*. Sonodynamic Therapy with anticancer micelles and high-intensity focused ultrasound in treatment of canine cancer. Front Pharmacol 2019;10:545.
26. Isard PF, Mentek M, Clément D, Béglé A, Romano F, Aptel F, *et al*. High intensity focused ultrasound cyclocoagulation in dogs with primary glaucoma: A preliminary study. Open Vet J 2018;8:305-12.
27. Lü F, Huang W, Benditt DG. A feasibility study of noninvasive ablation of ventricular tachycardia using high-intensity focused ultrasound. J Cardiovasc Electrophysiol 2018;29:788-94.
28. Yao Y, Qian J, Rong S, Huang Y, Xiong B, Yang G, *et al*. Cardiac denervation for arrhythmia treatment with transesophageal ultrasonic strategy in canine models. Ultrasound Med Biol 2019;45:490-9.
29. Rong S, Woo K, Zhou Q, Zhu Q, Wu Q, Wang Q, *et al*. Septal ablation induced by transthoracic high-intensity focused ultrasound in canines. J Am Soc Echocardiogr 2013;26:1228-34.
30. Zheng M, Shentu W, Chen D, Sahn DJ, Zhou X. High-intensity focused ultrasound ablation of myocardium *in vivo* and instantaneous biological response. Echocardiography 2014;31:1146-53.
31. Okumura Y, Kolasa MW, Johnson SB, Bunch TJ, Henz BD, O'Brien CJ, *et al*. Mechanism of tissue heating during high intensity focused ultrasound pulmonary vein isolation: Implications for atrial fibrillation ablation efficacy and phrenic nerve protection. J Cardiovasc Electrophysiol 2008;19:945-51.
32. Chen S, Ling Z, Yin Y, Li C, Zhang B, Zrenner B, *et al*. The comparison of epicardial focused ultrasound circumferential pulmonary vein ablation and BOX ablation--results from experimental acute atrial fibrillation. J Interv Card Electrophysiol 2012;34:153-9.
33. Wang Q, Guo R, Rong S, Yang G, Zhu Q, Jiang Y, *et al*. Noninvasive renal sympathetic denervation by extracorporeal high-intensity focused ultrasound in a pre-clinical canine model. J Am Coll Cardiol 2013;61:2185-92.
34. Shi B, Zhu H, Liu YJ, Lü L, Jin CB, Ran LF, *et al*. Experimental studies and clinical experiences on treatment of secondary hypersplenism with extracorporeal high-intensity focused ultrasound. Ultrasound Med Biol 2012;38:1911-7.
35. Leoci R, Aiudi G, Silvestre F, Lissner EA, Marino F, Lacalandra GM. Therapeutic ultrasound as a potential male dog contraceptive: Determination of the most effective application protocol. Reprod Domest Anim 2015;50:712-8.
36. Roberts WW, Wright EJ, Fried NM, Nicol T, Jarrett TW, Kavoussi LR, *et al*. High-intensity focused ultrasound ablation of the epididymis in a canine model: A potential alternative to vasectomy. J Endourol 2002;16:621-5.
37. Yiannakou M, Menikou G, Yiallouras C, Ioannides C, Damianou C. MRI guided focused ultrasound robotic system for animal experiments. Int J Med Robot 2017; 13:e1804.
38. Yiannakou M, Trimikliniotis M, Yiallouras C, Damianou C. Evaluation of focused ultrasound algorithms: Issues for reducing pre-focal heating and treatment time. Ultrasonics 2016;65:145-53.
39. Menikou G, Damianou C. Acoustic and thermal characterization of agar based phantoms used for evaluating focused ultrasound exposures. J Ther Ultrasound 2017;5:14.